Fast generation of entanglement in Bosonic Josephson Junctions

Giacomo Sorelli, Luca Pezzè, and Augusto Smerzi
QSTAR, INO-CNR and LENS, Largo Enrico Fermi 2, I-50125 Firenze, Italy
(Dated: November 6, 2015)

We use an exact quantum phase model to study the dynamical generation of particle-entanglement in a system composed by two weekly-coupled and interacting Bose-Einstein condensates. We show that linear coupling can accelerate the creation of entanglement with respect to the well known one-axis twisting model where coupling is absent. This provides an analytical understanding of the recent experimental results of W. Müssel et al. *Phys. Rev. A* **92**, 023603 (2015).

arXiv:1511.01835v1 [quant-ph] 5 Nov 2015

I. INTRODUCTION

The notion of entanglement was introduced by Schrödinger, more than sixty years ago [1] as a reaction to the Einstein-Podolski-Rosen paradox [2]. Early experiments performed with photons and ions have focused on the creation and demonstration of entanglement between two quantum-mechanical objects. Thanks to the experimental capabilities developed in the last twenty years, it has been possible to create entanglement between a large number of parties. Many-particle entanglement up to ten distinguishable parties has been demonstrated with photons [3, 4] and ions [5, 6], and up to hundreds indistinguishable parties with neutral atoms [7, 8]. From a foundational viewpoint, entanglement between several systems can be important to study the quantum-to-classical transition. It is also an ingredient of quantum technologies as, for instance, quantum metrology [9, 10]. For both purposes, it is desirable to create highly entangled states [11, 12]. However, the creation of large entanglement is challenged by unavoidable decoherence sources in common experiments. It is thus crucial to develop protocols creating entanglement on the fastest time scales as possible.

In this manuscript, we study the dynamical creation of entanglement in a bosonic Josephson junction (BJJ) made of two weakly-coupled and interacting Bose-Einstein condensates (BECs). The generation of multi-particle entanglement is due to atom-atom interactions in the condensate and it is accelerated by a linear mode-coupling that, alone, cannot create entanglement. The generation of entanglement in this system has been theoretically investigated [13–15] and experimentally observed [7, 16]. Analytical results are available in the weak interaction limit [15] and short time scales [14]. In particular, Ref. [14] has shown that linear coupling does not provide, in the early dynamics, any advantage on the creation of entanglement with respect to the one-axis twisting [17], where the linear coupling is not present. However, a difference between the models does exist, as shown in a recent experiment [16]. An analytical study covering the different interaction-versus-tunneling regimes and explaining the experimental findings is still missing.

Here we study the BJJ dynamics within an an exact quantum phase model (EQMP) first introduced in Ref. [18] and use the quantum Fisher information as entanglement witness. The analysis is extended to sufficiently long times so to observe a substantial difference between the BJJ dynamics and the one-axis twisting dynamics. Our results reveal that the claim of Ref. [14] are due to the short time scale considered and provide a guideline to understand recent experimental observations [7, 16]. The approximations used to solve the EQPM dynamics fail in the long-time limit where the system shows the onset of a Schrödinger cat state, as first discussed in [13].

The manuscript is organized as follows. We first introduce the EQPM and relevant multi-particle entanglement witnesses. In section III we present the dynamical generation of entanglement when the initial state is a coherent spin state pointing in the negative direction of the x-axis of the Bloch sphere. This situation corresponds to the unstable regime of the mean field dynamics [19, 20] and it is the working condition of the experiments [7, 16]. In section IV we draw a direct comparison with the one-axis twisting dynamics. We complete our study in Sec. V with the analysis of the dynamical generation of entanglement when the system is prepared in a coherent spin state pointing in the positive x-axis of the Bloch sphere, corresponding to the the fixed stable point of the mean field dynamics

II. TWO-MODE DYNAMICS OF INTERACTING BOSONS

A system composed by two weakly-coupled interacting Bose gases is generally described by the two-mode Hamiltonian [19, 21–24],

$$\hat{H} = \hbar\chi \hat{J}_z^2 - \hbar\Omega \hat{J}_x; \tag{1}$$

where Ω accounts for coupling among the a and b modes, and χ is a parameter related to the particle-particle interaction. Here,

$$\hat{J}_x = \frac{\hat{a}^\dagger\hat{b} + \hat{b}^\dagger\hat{a}}{2}, \quad \hat{J}_y = \frac{\hat{a}^\dagger\hat{b} - \hat{b}^\dagger\hat{a}}{2i}, \quad \text{and} \quad \hat{J}_z = \frac{\hat{a}^\dagger\hat{a} - \hat{b}^\dagger\hat{b}}{2}$$

are pseudo-spin operators satisfying the commutation relation $[\hat{J}_l, \hat{J}_n] = i\epsilon_{lnm}\hat{J}_m$, where ϵ_{lnm} is the Levi-Civita symbol, and $\hat{a}$ and $\hat{b}$ are mode annihilator operators. The model (1) can be realized in a physical system employing either external (e.g. a double-well trapping potential) or internal (e.g. two hyperfine atomic states) degrees of freedom of an atomic Bose-Einstein condensate.

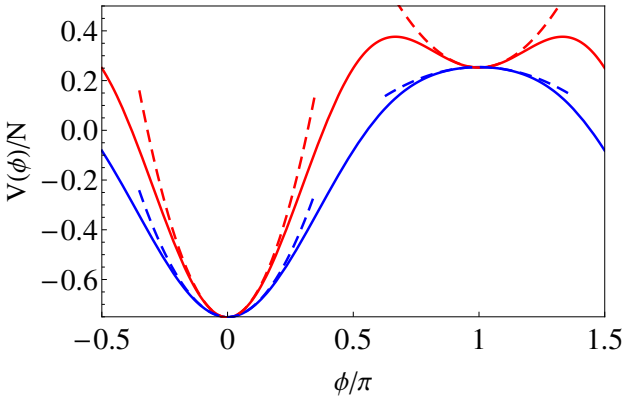

Figure 1. (color online) Effective phase potential $V(\phi)$ (solid lines), Eq. (5) normalized by N in the limit $N \gg 1$. Different lines refer to different values of Λ: the red line is for $\Lambda = 0.5$ while the blue one is for $\Lambda = 1.5$. Dashed lines are the harmonic oscillator approximation in the nearby of $\phi = 0$ and $\phi = \pi$.

A. Exact quantum phase model

Equation (1) can be studied within the exact quantum phase model (EQPM) [18]. It consists in expanding a general quantum state of the two-mode system,

$$|\psi\rangle = \int_{-\pi}^{\pi} \frac{\mathrm{d}\phi}{2\pi} \Psi(\phi)|\phi\rangle, \tag{2}$$

on the overcomplete basis of Bargmann states [25],

$$|\phi\rangle = \sum_{n=-N/2}^{N/2} \frac{e^{in\phi}}{\sqrt{\left(\frac{N}{2}+n\right)!\left(\frac{N}{2}-n\right)!}} \left|\frac{N}{2}+n\right\rangle_a \left|\frac{N}{2}-n\right\rangle_b.$$

Here $|N/2+n\rangle_a|N/2-n\rangle_b$ indicates a Fock states of $N/2+n$ particles in mode a and $N/2-n$ particles in mode b, where N is the total number of particles. In this representation we can express the action of spin operators on the state $|\psi\rangle$ in terms of differential operators acting on $\Psi(\phi,t)$. Explicit expressions for the first and second moments of the spin operators are reported in the Appendix A. We can write the Hamiltonian (1) as [18]

$$\hat{H}|\psi(t)\rangle = \int_{-\pi}^{\pi} \frac{\mathrm{d}\phi}{2\pi} \left[\mathcal{H}_\phi \psi(\phi,t)\right] e^{\frac{N}{2\Lambda}\cos\phi}|\phi\rangle \tag{3}$$

where $\Lambda = \frac{N\chi}{\Omega}$ is the ratio between interaction and tunneling. In the following we focus to the case of repulsive interaction $\Lambda > 0$. Our analysis generalizes to attractive interaction $\Lambda < 0$ via the mapping $t \to -t$ and $\phi \to \phi + \pi$. The Hamiltonian $\mathcal{H}_\phi$ is given by

$$\mathcal{H}_\phi = \Omega\left(-\frac{\Lambda}{N}\frac{\partial^2}{\partial\phi^2} + V(\phi)\right). \tag{4}$$

where

$$V(\phi) = -\left(\frac{N+1}{2}\right)\cos\phi - \frac{N}{8\Lambda}\cos 2\phi \tag{5}$$

is an effective potential. The time evolution of the system can thus be mapped on the dynamics of a fictitious wave-packet evolving in the potential $V(\phi)$. In Fig. 1 we show $V(\phi)$ for different values of Λ. While the potential is always confining in the nearby of $\phi = 0$, close to $\phi = \pi$ the potential $V(\phi)$ becomes a repulsive inverted parabola when $\Lambda > N/(N+1)$. The different behavior of the effective potential close to $\phi = 0$ and π has direct implications in the creation of many-particle entanglement, as discussed below. It should be noticed that there is no approximation leading to Eq. (3): the EQPM is exact for any number of particles. Another advantage of the model is that the dynamics of the many-body state, $i\hbar\frac{\partial|\psi(t)\rangle}{\partial t} = \hat{H}|\psi(t)\rangle$, can be studied in terms of the Schrödinger equation

$$i\hbar\frac{\partial\psi(\phi,t)}{\partial t} = \mathcal{H}_\phi\psi(\phi,t) \tag{6}$$

describing the motion of an effective wave packet in the potential (5). Within the harmonic (attractive or repulsive) oscillator approximation in the nearby of $\phi = 0, \pi$, the complete dynamics in the phase representation can be analytically studied using a Gaussian wave function $\psi(\phi,t)$. Details on the use of the Gaussian approximation and on the computation of relevant expectation values can be found in Appendix B. As a main drawback of the EQPM, the Bargmann basis is overcomplete, which makes the calculation of expectation values of a generic observables $\hat{A}$

$$\langle\psi|\hat{A}|\psi\rangle = \int_{-\pi}^{\pi}\frac{\mathrm{d}\theta}{2\pi}\int_{-\pi}^{\pi}\frac{\mathrm{d}\phi}{2\pi}\Psi(\theta,t)^* A(\phi,t)\Psi(\phi,t)\langle\theta|\phi\rangle, \tag{7}$$

and inner product

$$\langle\psi|\psi'\rangle = \int_{-\pi}^{\pi}\frac{\mathrm{d}\theta}{2\pi}\int_{-\pi}^{\pi}\frac{\mathrm{d}\phi}{2\pi}\Psi(\theta,t)^*\Psi'(\phi,t)\langle\theta|\phi\rangle, \tag{8}$$

non-local in phase, with the non standard inner product $\langle\theta|\phi\rangle = (2^N/N!)\cos^N[(\theta-\phi)/2]$. This term is crucial to cut Fourier contributions with frequency smaller than $1/N$. For large N, we will use the approximation $\cos^N[(\theta-\phi)/2] \sim \exp[-N(\theta-\phi)^2/8]$, and expect to obtain correct results modulo contributions of the order $1/N$. The factor $e^{\frac{N}{2\Lambda}\cos\phi}$ in Eq. (3) is crucial to obtain a correct dynamics. It can be conveniently approximated as $e^{-\frac{N}{4\Lambda}\phi^2}$ in the nearby of $\phi = 0$ and as $e^{\frac{N}{4\Lambda}(\phi+\pi)^2}$ around $\phi = \pi$.

In a previous work [26], the EQPM has been used to study the ground state of Eq. (1) for repulsive interaction. Here we consider the dynamical generation of entanglement starting from separable states

$$|\vartheta,\varphi\rangle_N = \left(\hat{a}^\dagger\cos\frac{\vartheta}{2} + \hat{b}^\dagger e^{i\varphi}\sin\frac{\vartheta}{2}\right)^N|\mathrm{vac}\rangle, \tag{9}$$

where $|\mathrm{vac}\rangle$ is the vacuum. Equation (9) is generally indicated as coherent spin state (CSS) [27] and is given by all N qubits pointing along the same direction $\mathbf{s} = \{\sin\vartheta\cos\varphi, \sin\vartheta\sin\varphi, \cos\vartheta\}$ (called the mean spin direction) in the Bloch sphere, where $0 \le \vartheta \le \pi$ and $-\pi \le \varphi < \pi$.

The CSS has collective spin mean values $\langle \hat{J}_{\mathbf{s}} \rangle = N/2$ and $\langle \hat{J}_{\perp} \rangle = 0$, and variances $(\Delta \hat{J}_{\mathbf{s}})^2 = 0$ and $(\Delta \hat{J}_{\perp})^2 = N/4$, where $\perp$ indicates an arbitrary direction orthogonal to the mean spin direction.

It is worth recalling that there are alternative approaches to the EQPM to study Eq. (1), besides the numerical exact diagonalization. A well explored method is a semiclassical approximation in number space [28, 29] that was used in Ref. [14] to discuss the generation of many-particle entanglement in the BJJ.

B. Entanglement, spin-squeezing and quantum Fisher information

To witness and quantify the creation of particle entanglement we calculate the spin-squeezing parameter

$$\xi^2 = \frac{N(\Delta \hat{J}_{\mathbf{n}_3})^2}{\langle \hat{J}_{\mathbf{n}_1} \rangle^2} \tag{10}$$

and the quantum Fisher information

$$F_Q[\hat{J}_{\mathbf{n}_2}] = 4(\Delta \hat{J}_{\mathbf{n}_2})^2, \tag{11}$$

where $\mathbf{n}_1$, $\mathbf{n}_2$ and $\mathbf{n}_3$ are three mutually orthogonal directions. The criteria [30, 31]

$$\xi^2 < 1 \tag{12}$$

and [9]

$$\zeta^2 = \frac{N}{F_Q[\hat{J}_{\mathbf{n}_2}]} < 1. \tag{13}$$

are sufficient for entanglement between the N particles, i.e. the state of the system cannot be written as $\hat{\rho} = \sum_k q_k \hat{\rho}_k^{(1)} \otimes \hat{\rho}_k^{(2)} \otimes ... \otimes \hat{\rho}_k^{(N)}$, where $q_k > 0$ and $\hat{\rho}_k^{(j)}$ is the state of the jth particle. The conditions (12) and (13) have an operational meaning. Equation (12) recognizes all the entangled spin-squeezed states that can be used to sense a rotation $e^{-i\theta \hat{J}_{\mathbf{n}}}$ with a sensitivity overcoming the shot-noise limit $\Delta\theta = 1/\sqrt{mN}$, where m accounts for the repetition of independent measurements. Since the highest attainable interferometric phase sensitivity is limited by the quantum Cramér-Rao lower bound, $\Delta\theta_{\rm QCR} = 1/\sqrt{mF_Q[\hat{J}_{\mathbf{n}_2}]}$ [32, 33], Eq. (13) detects all the entangled states that can be used to overcome the shot-noise limit when sensing the rotation $e^{-i\theta \hat{J}_{\mathbf{n}_2}}$. In particular, the inequality

$$\zeta^2 \leq \xi^2 \tag{14}$$

holds [9] and thus the QFI recognizes the full class of states (including the spin-squeezed ones) useful to overcome the shot-noise limit. The highest value of the QFI is $F_Q[\hat{J}_{\mathbf{n}_2}] = N^2$, which corresponds to the so called Heisenberg limit of phase sensitivity, $\Delta\theta_{\rm HL} = 1/\sqrt{m}N$, representing the ultimate bound for phase estimation [10].

In the following we compute ξ^2 and ζ^2 for initial CSS pointing on the $\mathbf{x}$-axis and evolving according to Eq. (1). These states are characterized by $\langle \hat{J}_{\mathbf{z}} \rangle = \langle \hat{J}_{\mathbf{y}} \rangle = 0$ at every time. Therefore, the optimal spin-squeezing and QFI are obtained by minimizing (to calculate the spin-squeezing) or to maximizing (to calculate the QFI) the spin variance on the $\mathbf{y} - \mathbf{z}$ plane. This is done by computing the eigenvalues

$$\lambda_{\pm} = \frac{1}{2}\left[\gamma_{zz} + \gamma_{yy} \pm \sqrt{(\gamma_{zz} - \gamma_{yy})^2 + (2\gamma_{yz})^2}\right]. \tag{15}$$

(with $\lambda_+ > \lambda_-$) of the covariance matrix

$$\gamma_{ij} = \frac{2\langle \{\hat{J}_i, \hat{J}_j\} \rangle}{N}, \tag{16}$$

where $i, j = \mathbf{y}, \mathbf{z}$, and curly brackets stands for the anti-commutator between the two angular momenta. Note that $\gamma_{zz} = 4(\Delta \hat{J}_{\mathbf{z}})^2/N$ and $\gamma_{yy} = 4(\Delta \hat{J}_{\mathbf{y}})^2/N$. The optimal values of ξ^2 and ζ^2 are thus given by

$$\xi^2_{\rm opt} = \frac{N^2 \lambda_-}{4\langle \hat{J}_{\mathbf{x}} \rangle^2}, \quad \text{and} \quad \zeta^2_{\rm opt} = \frac{1}{\lambda_+}. \tag{17}$$

III. ENTANGLEMENT GENERATION AROUND $\phi = \pi$

We focus here on the generation of entanglement starting from the CSS

$$|\pi/2, \pi\rangle_N = \left(\frac{\hat{a}^\dagger - \hat{b}^\dagger}{\sqrt{2}}\right)^N |{\rm vac}\rangle, \tag{18}$$

polarized along the negative x-axis (it is the eigenstate of $\hat{J}_x$ with minimum eigenvalue $-N/2$). For $\phi \approx \pi$, Eq. (4) becomes the Hamiltonian of a harmonic oscillator of square frequency

$$\frac{\omega_\pi^2}{\Omega^2} = 1 - \Lambda\left(1 + \frac{1}{N}\right). \tag{19}$$

Equation (19) is positive [corresponding to a confining effective potential $V(\phi)$] for $\Lambda < N/(N+1)$ and negative [corresponding to a repulsive $V(\phi)$] for $\Lambda > N/(N+1)$, see Fig. (1). The change of sign of ω_π^2 is directly linked to the onset on instability of the corresponding mean-field fixed point [19, 20]. We further define $\omega_\pi = |\sqrt{\omega_\pi^2}|$. To study the quantum dynamics within the EQPM we use the Gaussian wave function

$$\psi(\phi, t) = e^{-[a_\pi(t) + i b_\pi(t)](\phi - \pi)^2}, \tag{20}$$

where

$$a_\pi(t) = \frac{\frac{N\omega_\pi^2}{2\Lambda^2}\alpha_\pi}{\frac{\omega_\pi^2}{\Lambda^2} + \alpha_\pi^2 + \left(\frac{\omega_\pi^2}{\Lambda^2} - \alpha_\pi^2\right)\cos(2\omega_\pi t)} - \frac{N}{4\Lambda}, \tag{21a}$$

$$b_\pi(t) = -\frac{N\omega_\pi}{4\Lambda}\frac{\left(\frac{\omega_\pi^2}{\Lambda^2} - \alpha_\pi^2\right)\sin(2\omega_\pi t)}{\frac{\omega_\pi^2}{\Lambda^2} + \alpha_\pi^2 + \left(\frac{\omega_\pi^2}{\Lambda^2} - \alpha_\pi^2\right)\cos(2\omega_\pi t)}, \tag{21b}$$

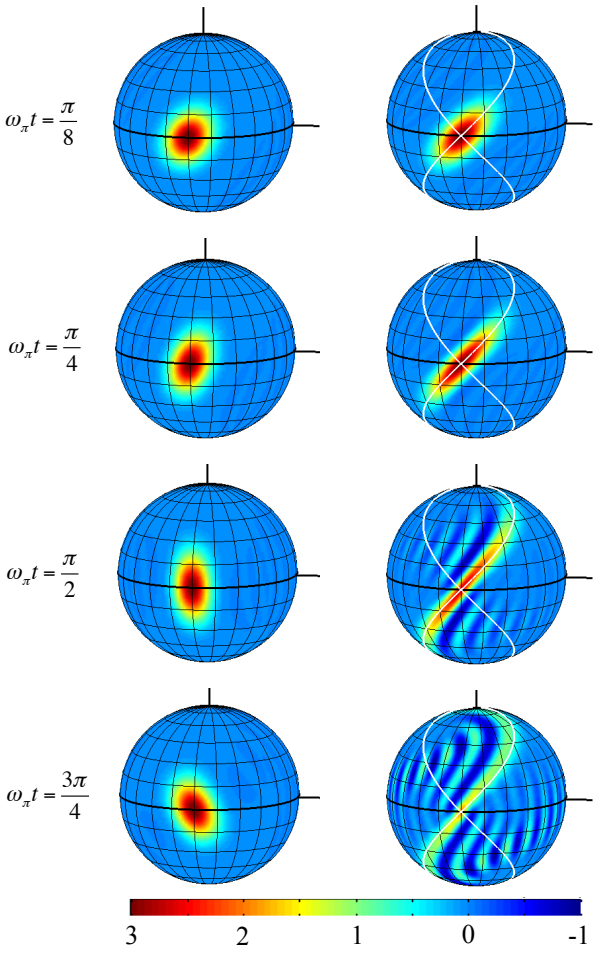

Figure 2. (color online) Wigner distributions (normalized to one) of the states obtained from the dynamical evolution of Eq. (18) in the case $\Lambda = 0.5$ (left column) and $\Lambda = 2$ (right column). Different rows correspond to different evolution times. The thick white line is the separatrix of the mean-field dynamics. Here $N = 30$.

with $\alpha_\pi = \left(\frac{1+\omega_\pi(\Lambda_0)}{\Lambda_0} + \frac{1}{\Lambda}\right)$ and $\omega_\pi(\Lambda_0)$ is the frequency Eq. (19) computed with an interaction parameter Λ_0. Mean spin moments are calculated taking the limit $\Lambda_0 \to 0$, see further discussion in Appendix B. We also consider $N \gg 1$ and neglect terms of the order $1/N$. We emphasize that, within the approximation (20), we cannot distinguish between the QFI and spin-squeezing: $\zeta^2_{\rm opt} = \xi_{\rm opt}$ in our analytical calculations.

Stable regime, $\Lambda < N/(N+1)$. In the stable regime, the dynamics is characterized by a periodic generation of phase squeezing. Figure 2 shows the Wigner distribution on the Bloch sphere [34] plotted at different evolution times. The initial isotropic Wigner distribution of the CSS deforms in time, becoming elliptic and reaching its maximum squeezing along the y-axis (phase squeezing, see below). A calculation of Eq. (16) with the Gaussian state (20) gives

$$\gamma_{zz} = \frac{1}{2(\Lambda-1)}\left(\Lambda + \Lambda\cos 2\omega_\pi t - 2\right), \tag{22a}$$

$$\gamma_{yy} = \frac{1}{2}\left(2 - \Lambda + \Lambda\cos 2\omega_\pi t\right), \tag{22b}$$

$$\gamma_{yz} = \gamma_{zy} = -\frac{2\Lambda}{\sqrt{1-\Lambda}}\sin 2\omega_\pi t, \tag{22c}$$

and

$$\frac{2\langle \hat{J}_x\rangle}{N} = -1 + \frac{1}{4N}\frac{\Lambda^2}{\Lambda-1}\left(\cos 2\omega_\pi t - 1\right). \tag{23}$$

These expectation values are used to calculate $\zeta^2_{\rm opt}$. In Fig. 3 we show $\zeta^2_{\rm opt}$ as a function of time and we compare them with the numerical results obtained from the exact diagonalization of Eq. (1). The upper panel is obtained for $\Lambda = 0.5$ and shows periodic oscillations of $\xi^2_{\rm opt}$ and $\zeta^2_{\rm opt}$. Indeed, a non-zero value of the non-diagonal terms of the covariance matrix γ_{yz} varying in time implies that $\xi^2_{\rm opt}$ and $\zeta^2_{\rm opt}$ are minimized along a direction in the **yz** plane that varies during the evolution. For moderate values of Λ sufficiently far from the critical $\Lambda = 1$, our Gaussian approximation (20) well reproduces numerical results. We find a periodic generation of entanglement [15], see Fig. 3, with minima at $2\omega_\pi t = n\pi$, with n an integer number, reaching (in time) a minimum value

$$\zeta^2_{\rm min} = 1 - \Lambda. \tag{24}$$

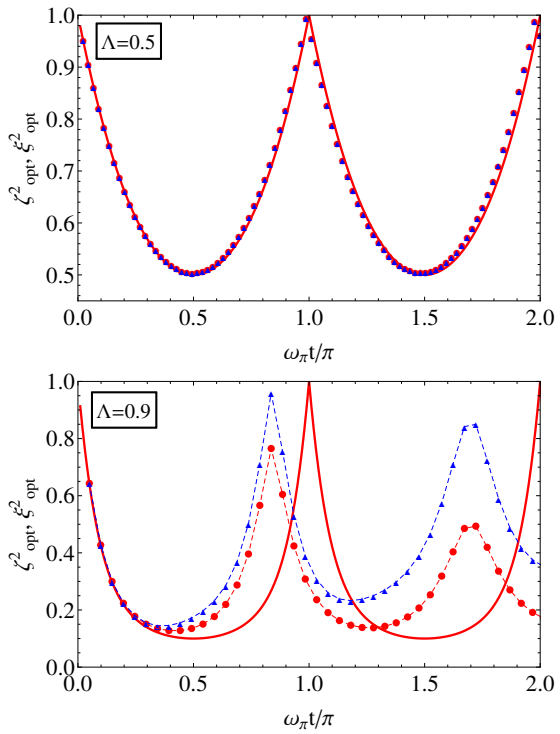

Figure 3. (color online) Time evolutions of $\zeta^2_{\rm opt}$ (red points) and $\xi^2_{\rm opt}$ (blue triangles) along the direction of maximal entanglement computed via exact numerical calculation. The solid red line is out analytical calculation of $\zeta^2_{\rm opt}$. The two panels are obtained for different values of Λ and $N = 200$, with the initial state Eq. (18).

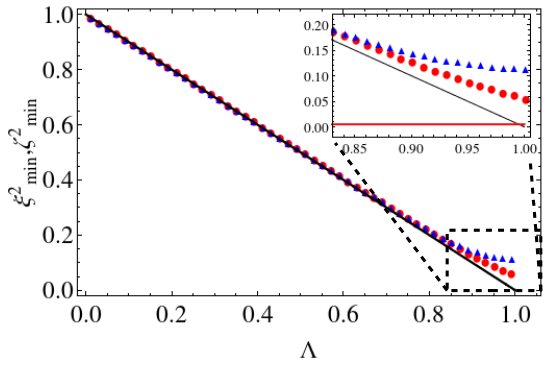

Figure 4. (color online) Comparison between the minima (in time) of $\zeta^2_{\rm opt}$ (red dots) and $\xi^2_{\rm opt}$ (blue dots) computed numerically and the analytical prediction Eq. 24 (black line). The inset is a zoom around $\Lambda = 1$. The horizontal red line is the Heisenberg limit $\zeta^2 = 1/N$. Here $N = 200$.

As expected, due to the relative weak nonlinearity, we obtain a modest generation of entanglement. Approaching $\Lambda = 1$ the Gaussian approximation reproduces the numerical findings only for very short times $t \ll \pi/\omega_\pi$, where $\xi^2_{\rm opt} \simeq \zeta^2_{\rm opt}$, as shown in the lower panel of Fig. 3. Anharmonic effects in the potential $V(\phi)$ become important and the oscillations of $\xi^2_{\rm opt}$ and $\zeta^2_{\rm opt}$ quickly damp.

In Fig. 4 we plot the minimum (in time) value of $\xi^2_{\rm opt}$ and $\zeta^2_{\rm opt}$ as a function of Λ. The solid line is Eq. (24), while symbols are numerical results. We see that the maximal generation of entanglement depends on Λ and Eq. (24), predicting an unphysical $\zeta^2_{\rm min} \to 0$ for $\Lambda \to 1$ and finite N (which corresponds to a diverging QFI), fails when approaching the critical value. The region where our approximation predicts the correct minima increase increasing the number of particles.

Unstable regime $\Lambda > N/(N+1)$. In the unstable regime, the quantum dynamics of the initial CSS (18) is quite different from the stable one. As shown in Fig. (2) for $\Lambda = 2$, the initial CSS symmetric Wigner distribution evolves quickly in a highly asymmetric ellipse, stretching along the separatrix of the mean-field dynamics. We thus expect to find a large generation of useful entanglement in this regime. For long times the state wraps around the mean-field fixed points at $\phi = \pi$ and $2\langle \hat{J}_z\rangle/N = \pm\sqrt{1+1/\Lambda^2}$ and large negative values of the Wigner function are obtained. In the unstable regime, the phase potential $V(\phi)$ is non-confining and the harmonic approximation works for relatively short times. We find

$$\gamma_{zz} \simeq \frac{1}{2(\Lambda-1)}\left(\Lambda + \Lambda\cosh 2\omega_\pi t - 2\right), \tag{25a}$$

$$\gamma_{yy} \simeq \frac{1}{2}\left(2 - \Lambda + \Lambda\cosh 2\omega_\pi t\right), \tag{25b}$$

$$\gamma_{yz} = \gamma_{zy} \simeq -\frac{2\Lambda}{\sqrt{1-\Lambda}}\sinh 2\omega_\pi t, \tag{25c}$$

and

$$\frac{\langle \hat{J}_x\rangle}{N/2} \simeq -1 + \frac{1}{4N}\frac{\Lambda^2}{\Lambda-1}\left(\cosh 2\omega_\pi t - 1\right). \tag{26}$$

These equations predict an exponential change of γ_{ij}, which implies that the optimal squeezing direction does not change in time. The exponential growths (or decays) of the matrix elements of γ_{ij} suggest that the evolution will provide a fast generation of entanglement. It should be noticed that Eqs. (25) and (26) agree with those presented in [14] and obtained with a different method (in number space [28]) involving approximations similar to ours.

In Fig. 5 we plot the analytical $\zeta^2_{\rm opt}$ (red line) compared with the results of QFI (red dots) and spin squeezing (blue triangles) obtained from the exact numerical calculations of Eq. (1). The spin-squeezing parameter decreases until it reaches a minimum and then it starts growing: the quantum dynamics features a loss of spin-squeezing at relatively long times ($\omega_\pi t \approx \pi/2$) that is associated to the wrapping of the state [7] and, equivalently, the onset of strongly negative parts of the Wigner function, as shown in Fig. 2. On contrary ζ^2_{opt} keeps decreasing even after the spin-squeezing parameter reaches a minimum. The QFI is a more powerful witness of entanglement in this case. The analytical findings reproduce quite well the short time dynamics. The natural question is: how long does this agreement occur?

Let us expand the $\zeta^2_\pi \equiv \zeta^2_{\rm opt}$ in Taylor series for short time,

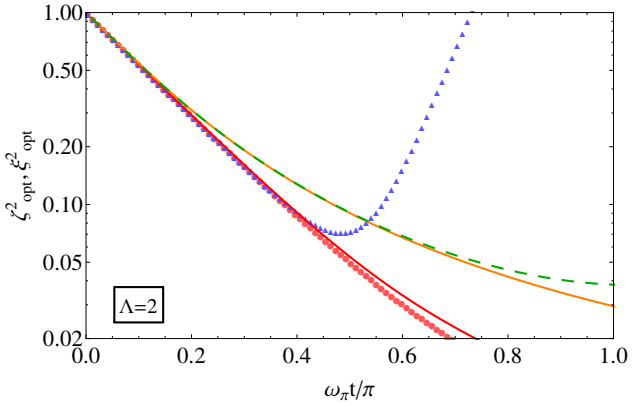

Figure 5. (color online) Time evolution of $\zeta^2_{\rm opt}$ (red points) and $\xi^2_{\rm opt}$ (blue triangles) compared to the analytical $\zeta^2_{\rm opt}$ (red line). The green dashed line and the orange line are respectively ξ^2_{opt} and ζ^2_{opt} for the one-axis twisting dynamics. Here $N = 200$.

$$\zeta_\pi^2 = 1 - N\chi t + \frac{N^2\chi^2}{2}t^2 - \frac{N^3\chi^3}{8}t^3 - \frac{1}{6}(\Lambda^2-\Lambda)\Omega^3 t^3 + \frac{1}{6}(\Lambda^3-\Lambda^2)\Omega^4 t^4 + O(N\chi t)^5, \tag{27}$$

where $\Omega \lesssim N\chi$. In Ref. [14] it was argued that only the linear term in Eq. (27) is accurate. Figure 6 shows that retaining only the linear term is overly conservative. There, we plot the different terms in Taylor expansion (27) compared with polynomial fits of the exact numerical diagonalization of Eq. (1) at the same order in time. We find an extremely good agreement, even for relatively large values of Λ, up, at least, to the fourth order in $N\chi t$. The disagreement between the numerics and the analytical coefficients of the Taylor expansion is of the order $1/N$ that, as discussed above, is the accuracy of our approximations. Retaining high-order terms in the Taylor expansion allows us to go beyond the results of Ref. [14] and perform a direct comparison between the unstable dynamics and the one-axis twisting dynamics (i.e. $\Omega = 0$, see below). One of the main results of Ref. [14] is that, to the first order in time, the unstable dynamics agrees with the one-axis twisting dynamics. Below, we show that a difference between the two dynamics can be appreciated when considering higher-order terms in Taylor expansion.

IV. COMPARISON WITH THE ONE-AXIS TWISTING DYNAMICS

One-axis twisting (OAT) is a benchmark model for studying the generation of spin-squeezed states [17, 35] and useful entanglement for quantum metrology [9]. The one-axis twisting Hamiltonian (along the z-axis, for example) is

$$\hat{H} = \hbar\chi \hat{J}_z^2, \tag{28}$$

and corresponds to the case $\Omega = 0$ in Eq. (1). It has been experimentally realized via particle-particle interactions in BECS [36–39]. For an initial state CSS on the equator of the Bloch sphere, $|\pi/2, \varphi\rangle_N$ one finds [17]

$$\frac{\langle \hat{J}_x \rangle}{N/2} = \cos^{N-1}\left(\frac{\chi t}{2}\right), \tag{29}$$

and

$$\lambda_\pm = \left\{1 + \frac{1}{4}(N-1)\left[A \pm \sqrt{A^2+B^2}\right]\right\}, \tag{30}$$

where $A = 1 - \cos^{N-2}(\chi t)$ and $B = 4\sin\left(\frac{\chi t}{2}\right)\cos^{N-2}\left(\frac{\chi t}{2}\right)$. From these equations we can readily calculate the optimized QFI $\zeta^2_{\rm OAT}$, using Eqs. (17). Expanding in Taylor series, we obtain

$$\zeta^2_{\rm OAT} = 1 - N\chi t + \frac{N^2\chi^2 t^2}{2} - \frac{N^3\chi^3 t^3}{8} + O(N\chi t)^5. \tag{31}$$

A direct comparison between Eq. (27) and Eq. (31) shows that unstable dynamics and one-axis twisting produce, up to second order in $N\chi t$, the same amount of useful entanglement. The leading difference appears in the third-order term:

$$\zeta^2_{\rm OAT} - \zeta^2_\pi = \frac{1}{6}\left(\Lambda^2 - \Lambda\right)\Omega^3 t^3 \tag{32}$$

which is larger than zero for all $\Lambda > 1$. We also notice that the fourth-order term in $N\chi t$ is missing in Eq. (31), while its is present in Eq. (27) and, being negative, it contributes to the generation of entanglement. We thus conclude that for relatively short times (up to $O(N\chi t)^5$, at least), the unstable regime of the BJJ dynamics produce more entanglement than one-axis twisting. This provides an analytical explanation of the recent experimental findings of Ref. [7, 16]. In order to understand when the difference in the dynamics introduced by the transverse linear term $\Omega\hat{J}_x$ is more relevant, we consider the ratio between the third-order coefficients in the power series of ζ_π and $\zeta_{\rm OAT}$:

$$R = 1 + \frac{4}{3}\left(\frac{1}{\Lambda} - \frac{1}{\Lambda^2}\right). \tag{33}$$

Maximizing this simple expression we find that the value of Λ for which the effect of the linear term is most relevant is $\Lambda = 2$. In panel (d) of Fig. 6 we compare our analytical prediction for R (line) with that obtained from exact numerical simulations (points). We obtain a very good agreement that confirms $\Lambda = 2$ as the optimal parameter for the quantum dynamics. It should be noticed that $\Lambda = 2$ is a special value in

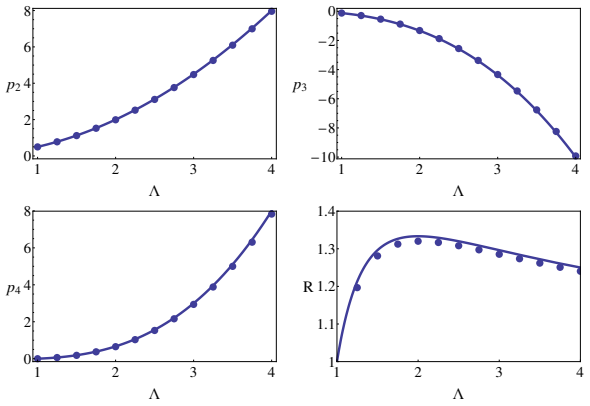

Figure 6. Panels (a), (b) and (c) show a comparison between analytical (solid line) and numerical (dots) coefficients in the Taylor series of ζ^2 for order two, three and four in $N\chi t$, respectively, as a function of Λ. Lines are obtained from Eq. (27): here $p_2 = \frac{\Lambda^2}{2}$, $p_3 = -\frac{\Lambda^3}{8} - \frac{\Lambda^2}{6} + \frac{\Lambda}{6}$ and $p_4 = \frac{1}{6}(\Lambda^3 - \Lambda^2)$. Dots are obtained from a polynomial fit of ζ^2 calculated with exact numerical diagonalization for $N = 200$. In panel (d) we show the ratio between the third order coefficient of the power series of ζ^2_π and of ζ^2_{OAT}. Dots are numerical results and the line is Eq. (33).

the mean-field BJJ dynamics: for $\Lambda = 2$ the separatrix passing through the point $\phi = \pi$ and $z = 2\langle \hat{J}_z \rangle / N = 0$ reaches its maximum extension passing the poles of the Bloch sphere, $\phi = \pi$ and $z = 2\langle \hat{J}_z \rangle / N = \pm 1$. In a sense, the mean-field bifurcation attains its maximum criticality. For $\Lambda > 2$ the mean-field dynamics features the onset of macroscopic self-trapping [19, 20]. Interestingly, $\Lambda = 2$ has been also identified in Ref. [13] as the optimal condition for the dynamical creation (on time scales $\chi t \approx \log(8N)/N$ much longer than those considered here) of maximally entangled states.

Finally, in Fig. 5 we compare $\zeta^2_{\rm opt}$ (red points) and $\xi^2_{\rm opt}$ for the unstable fixed-point dynamics (symbols) with the corresponding values for the OAT. The two different dynamics are equivalent for very short times. Yet, for sufficiently long times, when high order terms in the Taylor expansion (27) become relevant, the generation of entanglement in the bosonic Josephson junction is faster than in the OAT model. We can also notice that in both models, for times longer than those discussed in this work, there is a generation of states which are not spin-squeezed but are recognized as entangled by the QFI.

V. ENTANGLEMENT GENERATION AROUND $\phi = 0$

In the BJJ model, the most interesting quantum dynamics happens close to $\phi = \pi$. For completeness and comparison, here we study the quantum dynamics for a CSS

$$|\pi/2, 0\rangle_N = \left(\frac{\hat{a}^\dagger + \hat{b}^\dagger}{\sqrt{2}} \right)^N |\text{vac}\rangle, \tag{34}$$

polarized along the positive x-axis (it is the eigenvalue of $\hat{J}_x$ with maximum eigenvector $N/2$). An analytical study of the quantum dynamics close to the point $\phi \approx 0$ can be done substituting Eq. (4) with the Hamiltonian of a harmonic oscillator of square frequency

$$\omega_0^2 = 1 + \Lambda\left(1 + \frac{1}{N}\right). \tag{35}$$

The frequency ω_0^2 is always positive testifying that close to $\phi \approx 0$ we have an upward parabolic potential for every value of Λ, see Fig. 1.

In Fig. 7 we show the Wigner distribution plotted at different evolution time and Λ. For $\Lambda \lesssim 1$, the dynamics is periodic and quite similar to the one observed in Fig. 2 for $\phi = \pi$ and same value $\Lambda = 0.5$. The main difference here is the occurrence of squeezing of the initially isotropic distribution along the z-axis. Comparing the two columns we can see that increasing the value of Λ also the asymmetry of the Wigner distribution increases and negative parts appears. We study the quantum dynamics using the time-dependent wave function

$$\Psi(\phi, t) = e^{-(a_0(t) + i b_0(t)\phi^2}, \tag{36}$$

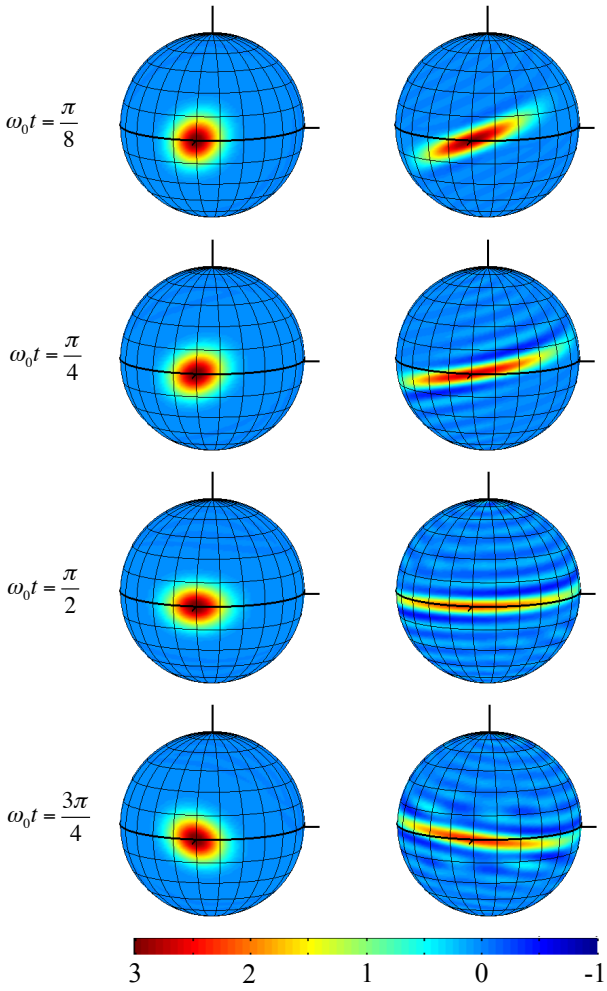

Figure 7. (color online) Wigner distributions (normalized to one) of the states obtained from the dynamical evolution of Eq. (34) in the case $\Lambda = 0.5$ (left column) and $\Lambda = N$ (right column). Different rows correspond to different evolution times. Here $N = 30$.

with parameters

$$a_0(t) = \frac{\frac{N\omega_0^2}{2\Lambda}\alpha_0}{\frac{\omega_0^2}{\Lambda^2} + \alpha_0^2 + \left(\frac{\omega_0^2}{\Lambda^2} - \alpha_0^2\right)\cos(2\omega_0 t)} - \frac{N}{4\Lambda} \tag{37a}$$

$$b_0(t) = \frac{N\omega_0}{4\Lambda} \frac{\left(\frac{\omega_0^2}{\Lambda^2} - \alpha_0^2\right)\sin(2\omega_0 t)}{\frac{\omega_0^2}{\Lambda^2} + \alpha_0^2 + \left(\frac{\omega_0^2}{\Lambda^2} - \alpha_0^2\right)\cos(2\omega_0 t)}, \tag{37b}$$

where $\alpha_0 = \left(\frac{1+\omega_0(\Lambda_0)}{\Lambda_0} - \frac{1}{\Lambda}\right)$, we obtain

$$\gamma_{zz} \simeq \frac{1}{2(1+\Lambda)}\left(2 + \Lambda + \Lambda\cos 2\omega_0 t\right), \tag{38a}$$

$$\gamma_{yy} \simeq \frac{1}{2}\left(2 + \Lambda - \Lambda\cos 2\omega_0 t\right), \tag{38b}$$

$$\gamma_{yz} = \gamma_{zy} \simeq \frac{\Lambda}{2\sqrt{1+\Lambda}}\sin 2\omega_0 t. \tag{38c}$$

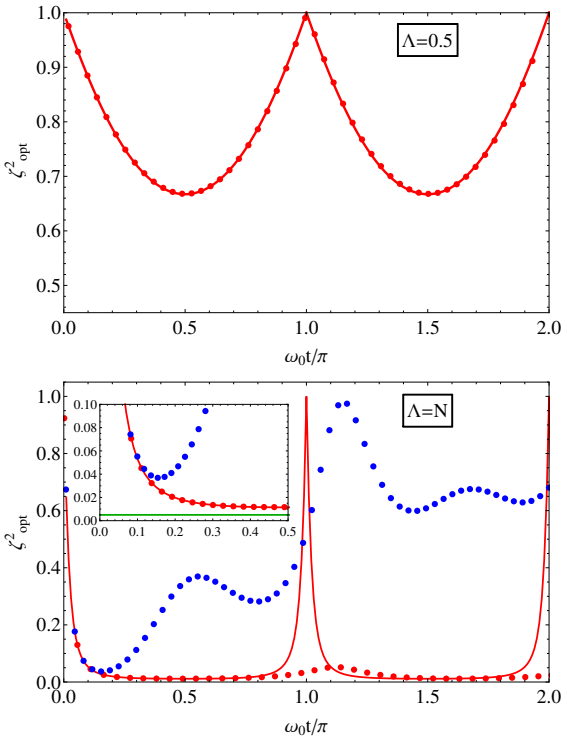

Figure 8. (color online) Time evolutions of $\zeta^2_{\rm opt}$ (red points) and $\xi^2_{\rm opt}$ (blue triangles) along the direction of maximal entanglement computed via exact numerical calculation. The solid red line is out analytical calculation of $\zeta^2_{\rm opt}$. The two panels are obtained for different values of Λ and $N = 200$, with the initial state Eq. (34).

giving the elements of the covariance matrix (16), and

$$\frac{\langle \hat{J}_x \rangle}{N/2} \simeq 1 + \frac{1}{4N}\frac{\Lambda^2}{1+\Lambda}\left(\cos 2\omega_0 t - 1\right). \tag{39}$$

These expressions agree with those computed in [14]. Like in the stable regime in the nearby of $\phi = \pi$ we have non-zero values of the non diagonal terms of the covariance matrix $\gamma_{yz} = \gamma_{zy}$ that varies in time telling us that $\xi^2_{\rm opt}$ and $\zeta^2_{\rm opt}$ are minimized along a direction in the **yz** plane that varies during the evolution. In Fig. 8 we show the oscillation of $\zeta^2_{\rm opt}$ for different values of Λ. We can see that in the regime $\Lambda \lesssim 1$ our approximation fits perfectly the exact numerical points.

The minima (in time) $\zeta^2_{\rm opt}$ are obtained for $2\omega_0 t = n\pi$, with n an integer number. The depth of these minima, at the zeroth order in $1/N$, is:

$$\xi^2_{min} \sim \zeta^2_{min} \sim \frac{1}{1+\Lambda} \tag{40}$$

According to this prediction, increasing Λ we have more and more entanglement. However, the approximations leading to Eq. (40) fail for $\Lambda \gg 1$. The lower panel of Fig. (8) shows the spin squeezing and the number of particles over the Fisher Information for $\Lambda = N$. Our analytical results follow the dynamical regime only for relatively short times $t \lesssim \pi/\omega_0$. For longer times we observe a net difference between the numerical $\xi^2_{\rm opt}$ and $\zeta^2_{\rm opt}$, corresponding to the onset of a negative Wigner function, see Fig. 7. In Fig. (9) we plot the minimum value (in time) of ξ^2_{opt} and ζ^2_{opt} as a function of Λ/N. We can see that the prediction of Eq. (40) fails when Λ becomes a significant fraction of the number of particles.

Finally, it is interesting to compare the stable and unstable dynamics for $\Lambda \gtrsim 1$. A Taylor expansion of $\zeta^2_0 \equiv \zeta^2_{\rm opt}$ for $N\chi t \ll 1$ gives

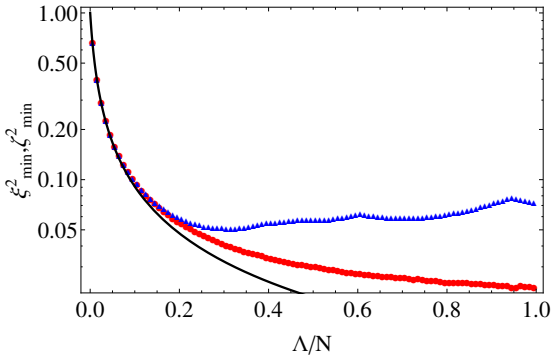

Figure 9. (color online) Comparison between the minima (in time) of $\zeta^2_{\rm opt}$ (blue dots) and $\xi^2_{\rm opt}$ computed numerically and the analytical prediction of Eq. 40 (black line).

$$\zeta^2_0 = 1 - N\chi t + \frac{N^2\chi^2 t^2}{2} - \frac{N^3\chi^3 t^3}{8} + \frac{1}{6}(\Lambda^2+\Lambda)\Omega^3 t^3 + \frac{1}{6}(\Lambda^3-\Lambda^2)\Omega^4 t^4 + O(N\chi t)^5, \tag{41}$$

where $\Omega \lesssim N\chi$. A direct comparison with Eq. (27) shows that all the terms in the Taylor expansion are equal except the sign of the Λ^2 factor in third order term, which is positive in Eq. (41) and negative in Eq. (27). For sufficiently short times, $\zeta^2_0 \leq \zeta^2_\pi$ for any value of Λ. We thus conclude that, at least in the short time dynamics, the unstable regime at $\phi = \pi$ is the optimal condition for generating entanglement useful for quantum interferometry.

VI. SUMMARY AND CONCLUSIONS

To summarize, we have studied the generation of entanglement useful for quantum metrology arising in the quantum dynamics of a bosonic Josephson Junction. The dynamics is characterized by particle-particle interaction and linear coupling. We have discussed different dynamical regime, depending of the initial polarization of the CSS and the

value of interaction-over-tunneling parameter Λ. The different regimes are well understood within a mean-field approximation [19, 20]. Analytical results for the QFI, valid for relatively short times, lead us to two important results: i) the dynamical generation of entanglement is fastest when the CSS points along the negative x-axis and $\Lambda = 2$, corresponding to maximum criticality in the mean-field unstable fixed point dynamics, and ii) in this regime, a direct comparison with the one-axis twisting dynamics [9, 17] shows that linear coupling accelerates the dynamical creation of entanglement. These findings help the understanding of recent experimental results [16] and can find direct application as a guideline to future experiments using an unstable dynamics to create large entanglement [40].

Appendix A: Action of collective spin operators in the EQPM

In this Appendix we report how the actions of the spin operators on a general two-mode state can be expressed in terms of differential operators acting on $\Psi(\phi, t)$ defined in (2).

$$\hat{J}_x|\psi\rangle = \int_{-\pi}^{\pi} \frac{\mathrm{d}\phi}{2\pi}|\phi\rangle \left[\sin\phi\frac{\partial}{\partial\phi} + \left(\frac{N}{2}+1\right)\cos\phi\right]\psi(\phi), \tag{A1a}$$

$$\hat{J}_y|\psi\rangle = \int_{-\pi}^{\pi} \frac{\mathrm{d}\phi}{2\pi}|\phi\rangle \left[\cos\phi\frac{\partial}{\partial\phi} - \left(\frac{N}{2}+1\right)\sin\phi\right]\psi(\phi), \tag{A1b}$$

$$\hat{J}_z|\psi\rangle = i\int_{-\pi}^{\pi} \frac{\mathrm{d}\phi}{2\pi}|\phi\rangle \frac{\partial}{\partial\phi}\psi(\phi). \tag{A1c}$$

$$\tag{A1d}$$

From the above expressions we can obtain the action of second-order operators such that:

$$\hat{J}_x^2|\psi\rangle = \int_{-\pi}^{\pi} \frac{\mathrm{d}\phi}{2\pi}|\phi\rangle \left[\sin^2\phi\frac{\partial^2}{\partial\phi^2} - \frac{N+3}{2}\sin(2\phi)\frac{\partial}{\partial\phi} + \left(\left(\frac{N}{2}+1\right)^2 - \left(\frac{N}{2}+2\right)\right)\cos^2\phi + \left(\frac{N}{2}-1\right)\right]\psi(\phi), \tag{A2a}$$

$$\hat{J}_y^2|\psi\rangle = \int_{-\pi}^{\pi} \frac{\mathrm{d}\phi}{2\pi}|\phi\rangle \left[\cos^2\phi\frac{\partial^2}{\partial\phi^2} - \frac{N+3}{2}\sin(2\phi)\frac{\partial}{\partial\phi} + \left(\left(\frac{N}{2}+1\right)^2 + \left(\frac{N}{2}+1\right)\right)\sin^2\phi - \left(\frac{N}{2}+1\right)\right]\psi(\phi), \tag{A2b}$$

$$\hat{J}_z^2|\psi\rangle = -\int_{-\pi}^{\pi} \frac{\mathrm{d}\phi}{2\pi}|\phi\rangle \frac{\partial^2}{\partial\phi^2}\psi(\phi), \tag{A2c}$$

$$\{\hat{J}_y, \hat{J}_z\}|\psi\rangle = i\int_{-\pi}^{\pi} \frac{\mathrm{d}\phi}{2\pi}|\phi\rangle \left[2\cos\phi\frac{\partial^2}{\partial\phi^2} - (N+3)\sin\phi\frac{\partial}{\partial\phi} - \left(\frac{N}{2}+1\right)\cos\phi\right]\psi(\phi). \tag{A2d}$$

Appendix B: Gaussian approximation

The exact representation of the coherent states (18) and (34) in the EQPM is a Dirac delta, but for the calculation is convenient to express everything in terms of Gaussian wave functions. To do so we will not consider as initial state an eigenstate of the Hamiltonian (1) with exactly $\Omega = 0$. We will instead initialize our EQPM dynamics with the Gaussian ground state of the harmonic approximation of (4) with an initial interaction parameter Λ_0. We then quench Λ to a different value and compute the evolution of the initial Gaussian into a harmonic potential. To investigate the dynamics of the CSS (18) we will simply shift the Gaussian ground state among $\phi = 0$ to $\phi = \pi$. In the end of all the calculations, for both the initial states, we will take the $\Lambda_0 \to 0$ limit of our results to recover the exact dependence by the coherent states.

Talking about ξ^2_{opt} and ζ^2_{opt} in Section II B we have pointed out that to compute these parameters we need to compute the expectation values of $\hat{J}_z^2$, $\hat{J}_y^2$, $\{\hat{J}_z, \hat{J}_z\}$ and $\hat{J}_x$. These operators can be expressed in the phase representation by equations (A1). In this Appendix we present the procedure we have used to obtain analytical expressions for their expectation values.

With our Gaussian approximation we have mapped the dynamics of the system into the well-known evolution of a Gaussian packet into a parabolic potential. Thus we have to deal with wave functions of the form

$$\psi(\phi, t) = \mathcal{N} e^{-(a(t)+ib(t))\phi^2}. \tag{B1}$$

Now we are going to compute the normalization constant $\mathcal{N}$:

$$\mathcal{N}^{-1} = \int_{-\pi}^{\pi}\int_{-\pi}^{\pi} \psi(\theta)^*\psi(\phi)\langle\theta|\phi\rangle d\theta d\phi = \int_{-\pi}^{\pi}\int_{-\pi}^{\pi} e^{-(a(t)-ib(t))\theta^2} e^{-(a(t)+ib(t))\phi^2} \cos^N\left(\frac{\theta-\phi}{2}\right) d\theta d\phi. \tag{B2}$$

This integral it is not easy to evaluate, but luckily can be approximated as a Gaussian integral that can be easily calculated. This can be done simply noticing that the second-order power series of the cosine to the nth power is equal to the one of a Gaussian of width $2/\sqrt{N}$,

$$\cos^N\left(\frac{\theta-\phi}{2}\right) = 1 - \frac{N(\theta-\phi)^2}{8} + o[(\theta-\phi)^3] \tag{B3a}$$

$$\exp\left(\frac{N(\theta-\phi)^2}{8}\right) = 1 - \frac{N(\theta-\phi)^2}{8} + o[(\theta-\phi)^3]. \tag{B3b}$$

Using thus the formulas for the generalized Gaussian integral we find

$$\mathcal{N}^{-1} = \frac{2\pi}{\sqrt{4(a^2+b^2)+Na}}. \tag{B4}$$

We have seen that, given an operator $\hat{A}$ acting on a quantum state of the many-particle system $|\psi\rangle$, we can always reduce it to a differential operator $\tilde{A}$ acting on the wave function $\psi(\phi,t)$. Thus the expectation value of $\hat{A}$ can be computed as

$$\langle\hat{A}\rangle = \int_{-\pi}^{\pi}\int_{-\pi}^{\pi} e^{-(a(t)-ib(t))\theta^2}\left[\tilde{A}e^{-(a(t)+ib(t))\phi^2}\right]\cos^N\left(\frac{\theta-\phi}{2}\right)d\theta d\phi. \tag{B5}$$

With the same procedure used for the normalization we can express (B5) in terms of Gaussian integrals. Thus, with these considerations and the expressions (A1), we can find approximated analytical expressions for all the expectation values needed to compute ξ and χ:

$$\langle\hat{J}_x\rangle = \frac{N}{2}e^{-\frac{8a+N}{8\mathcal{A}}}\left[\frac{(\mathcal{A}+a)\cos(b/\mathcal{A})+b\sin(b/\mathcal{A})}{\mathcal{A}}\right]; \tag{B6a}$$

$$\langle\hat{J}_z^2\rangle = \frac{N(a^2+b^2)}{\mathcal{A}}; \tag{B6b}$$

$$\langle\hat{J}_y^2\rangle = \frac{N}{8\mathcal{A}^2}\Big\{(N+1)\mathcal{A}^2 + aN\mathcal{A} - e^{-\frac{N+8a}{2\mathcal{A}}}\left[4b\left(\mathcal{A}N-\mathcal{B}\right)\sin(4b/\mathcal{A})+\right. \tag{B6c}$$
$$\left. + \left[(4a^2+4b^2)(4a+\mathcal{B}-N\mathcal{A}) - aN^2(\mathcal{A}+2a) + 4Nb^2\right]\cos(4b/\mathcal{A})\right]\Big\};$$

$$\langle\{\hat{J}_y,\hat{J}_z\}\rangle = \frac{N}{2}\frac{e^{-\frac{8a+N}{8\mathcal{A}}}}{\mathcal{A}^2}\left[-(4a(a^2+b^2)+Nb^2)\cos(b/\mathcal{A})+\right. \tag{B6d}$$
$$\left. +b(N\mathcal{A}-\mathcal{B})\sin(b/\mathcal{A})\right];$$

where we have defined

$$\mathcal{A} = 4(a^2+b^2)+aN, \tag{B7a}$$

$$\mathcal{B} = 4(a^2+b^2)-aN. \tag{B7b}$$

[1] E. Schrödinger, in Mathematical Proceedings of the Cambridge Philosophical Society, Vol. 31 (Cambridge Univ Press, 1935)

[2] A. Einstein, B. Podolsky, and N. Rosen, Physical review 47,777 (1935)

[3] X.-C. Yao, T.-X. Wang, P. Xu, H. Lu, G.-S. Pan, X.-H. Bao, C.-Z. Peng, C.-Y. Lu, Y.-A. Chen, and J.-W. Pan, Nature Photonics 6, 225 (2012).

[4] W.-B. Gao, C.-Y. Lu, X.-C. Yao, P. Xu, O. Gühne, A. Goebel, Y.-A. Chen, C.-Z. Peng, Z.-B. Chen, and J.-W. Pan, Nature Physics 6, 331 (2010).

[5] T. Monz, P. Schindler, J. T. Barreiro, M. Chwalla, D. Nigg, W. A. Coish, M. Harlander, W. Hänsel, M. Hennrich, and R. Blatt, Phys. Rev. Lett. 106, 130506 (2011).

[6] D. Leibfried, E. Knill, S. Seidelin, J. Britton, R. B. Blakestad, J. Chiaverini, D. B. Hume, W. M. Itano, J. D. Jost, C. Langer, et al., Nature 438, 639 (2005).

[7] H. Strobel, W. Muessel, D. Linnemann, T. Zibold, D. B. Hume, L. Pezzé, A. Smerzi, and M. K. Oberthaler, Science 345, 424 (2014).

[8] B. Lücke, M. Scherer, J. Kruse, L. Pezzé, F. Deuretzbacher, P. Hyllus, O. Topic, J. Peise, W. Ertmer, J. Arlt, L. Santos, A.

Smerzi, and C. Klempt, Science 334, 773 (2011).
[9] L. Pezzé and A. Smerzi, Phys. Rev. Lett. 102, 100401 (2009).
[10] V. Giovannetti, S. Lloyd, and L. Maccone, Phys. Rev. Lett. 96, 010401 (2006).
[11] P. Hyllus, W. Laskowski, R. Krischek, C. Schwemmer, W. Wieczorek, H. Weinfurter, L. Pezz'e, and A. Smerzi, Phys.Rev. A 85, 022321 (2012).
[12] G. Tóth, Phys. Rev. A 85, 022322 (2012).
[13] A. Micheli, D. Jaksch, J. I. Cirac, and P. Zoller, Phys. Rev. A 67, 013607 (2003).
[14] B. Juli á-Díaz, T. Zibold, M. K. Oberthaler, M. Melé-Messeguer, J. Martorell, and A. Polls, Phys. Rev. A 86, 023615 (2012).
[15] C. K. Law, H. T. Ng, and P. T. Leung, Phys. Rev. A 63, 055601 (2001).
[16] W. Muessel, H. Strobel, D. Linnemann, T. Zibold, B. Juli á-Díaz, and M. K. Oberthaler, Phys. Rev. A 92, 023603 (2015).
[17] M. Kitagawa and M. Ueda, Phys. Rev. A 47, 5138 (1993).
[18] J. R. Anglin, P. Drummond, and A. Smerzi, Phys. Rev. A 64, 063605 (2001).
[19] A. Smerzi, S. Fantoni, S. Giovanazzi, and S. R. Shenoy, Phys. Rev. Lett. 79, 4950 (1997).
[20] S. Raghavan, A. Smerzi, S. Fantoni, and S. Shenoy, Phys. Rev. A 59, 620 (1999).
[21] R. Gati and M. K. Oberthaler, Journal of Physics B: Atomic, Molecular and Optical Physics 40, R61 (2007).
[22] D. Ananikian and T. Bergeman, Phys. Rev. A 73, 013604 (2006).
[23] J. I. Cirac, M. Lewenstein, K. Mølmer, and P. Zoller, Phys. Rev. A 57, 1208 (1998).
[24] G. J. Milburn, J. Corney, E. M. Wright, and D. F. Walls, Phys. Rev. A 55, 4318 (1997).
[25] D. Walls and G. Milburn, Quantum Optics (Springer, New York, 1994).
[26] L. Pezzé, L. A. Collins, A. Smerzi, G. P. Berman, and A. R. Bishop, Phys. Rev. A 72, 043612 (2005).
[27] F. T. Arecchi, E. Courtens, R. Gilmore, and H. Thomas, Phys. Rev. A 6, 2211 (1972).
[28] V. S. Shchesnovich and M. Trippenbach, Phys. Rev. A 78, 023611 (2008).
[29] J. Javanainen and M. Y. Ivanov, Phys. Rev. A 59, 649 (1999).
[30] D. J. Wineland, J. J. Bollinger, W. M. Itano, F. L. Moore, and D. J. Heinzen, Phys. Rev. A 46, R6797 (1992).
[31] D. J. Wineland, J. J. Bollinger, W. M. Itano, and D. J. Heinzen, Phys. Rev. A 50, 67 (1994).
[32] C. W. Helstrom, Quantum Detection and Estimation Theory (Academic Press, 1976).
[33] S. L. Braunstein and C. M. Caves, Phys. Rev. Lett. 72, 3439 (1994).
[34] J. Dowling, G. S. Agarwal, and W. P. Schleich, Phys. Rev. A 49, 4101 (1994)
[35] A. Sørensen, L.-M. Duan, J. Cirac, and P. Zoller, Nature 409, 63 (2001).
[36] C. Gross, T. Zibold, E. Nicklas, J. Est'eve, and M. Oberthaler, Nature 464, 1165 (2010).
[37] M. Riedel, P. B öhi, Y. Li, T. H änsch, A. Sinatra, and P. Treutlein, Nature 464, 1170 (2010).
[38] C. F. Ockeloen, R. Schmied, M. F. Riedel, and P. Treutlein, Phys. Rev. Lett. 111, 143001 (2013).
[39] W. Muessel, H. Strobel, D. Linnemann, D. B. Hume, and M. K. Oberthaler, Phys. Rev. Lett. 113, 103004 (2014).
[40] C. D. Hamley, C. S. Gerving, T. M. Hoang, E. M. Bookjans, and M. S. Chapman, Nat. Phys. 8, 305 (2012).